View Article Online / Journal Homepage / Table of Contents for this issue
Dynamic Article Links

Journal of Materials Chemistry

Cite this: *J. Mater. Chem.*, 2012, **22**, 20482

www.rsc.org/materials

PAPER

Structure, defects and thermal stability of delithiated olivine phosphates†

Gene M. Nolis,[a] Fredrick Omenya,[a] Ruibo Zhang,[a] Bin Fang,[a] Shailesh Upreti,[a] Natasha A. Chernova,[a] Feng Wang,[b] Jason Graetz,[b] Yan-Yan Hu,[cd] Clare P. Grey[cd] and M. Stanley Whittingham*[ad]

Received 18th May 2012, Accepted 14th August 2012
DOI: 10.1039/c2jm33183g

Published on 15 August 2012. Downloaded by Florida State University on 7/18/2024 8:35:07 PM.

Studies of thermal decomposition mechanism of olivine $Fe_{1-y}Mn_yPO_4$ are reported here for inert (He), oxidizing (O_2) and oxidizing and moist (air) atmospheres using *in situ* X-ray diffraction and thermal gravimetric analysis with mass spectroscopy. The results indicate that the olivine structure is inherently stable up to at least 400 °C and $y = 0.9$ for particle size down to 50 nm. However, structural disorder and oxygen loss in the presence of reductive impurities, *e.g.* carbon and hydrogen, can occur as low as 250 °C for particles larger than 100 nm and at 150 °C for 50 nm particles. $Fe_{1-y}Mn_yPO_4$ is hygroscopic at high Mn contents, $y \geq 0.6$, and moisture exposure is more detrimental to its thermal stability than carbon or small particle size. Nano-$Fe_{1-y}Mn_yPO_4$ ($y > 0.7$) with particle size about 50 nm, when exposed to moisture, disorders at 150 °C and transforms to sarcopside phase by 300 °C, no matter whether the delithiation was done electrochemically or chemically. Contrary, under inert atmosphere the sample produced by chemical delithiation is stable up to 400 °C.

Introduction

A promising class of cathode materials for lithium-ion battery applications is the olivine-type $LiMPO_4$ (M = Fe, Mn) as they contain low-cost and abundant elements, as well as being environmentally benign.[1–5] Now commercially available, $LiFePO_4$ shows reversible lithium extraction/insertion at 3.45 V *vs.* Li/Li^+ with capacity approaching 170 A h kg^{-1}.[1,2] Interest in Mn-containing olivine phosphates results from the Mn^{2+}/Mn^{3+} redox potential at 4.1 V *vs.* Li/Li^+, leading to a higher theoretical energy density than its Fe counterpart.[1–5] However, $LiMnPO_4$ remains an inferior cathode material to $LiFePO_4$ due to its slower kinetics of Li extraction and insertion resulting from low ionic and electronic conductivities, large interface strain between Li-rich and Li-deficient phases and the metastable behaviour of its delithiated phase.[1–3]

The Li-deficient form of $LiFePO_4$, $FePO_4$, has many polymorphs, including olivine (o-), monoclinic, orthorhombic and trigonal (t-).[6–14] Arroyo y de Dompablo *et al.*, using density functional theory, demonstrated that t-$FePO_4$ is the thermodynamically stable phase at ambient pressure.[6] Phases other than t-$FePO_4$ transform to trigonal upon heating and, therefore, are considered metastable.[6–8,12–14] First principles calculations by Ong *et al.*[7] suggest a metastable decomposition route of o-$FePO_4$ involving Fe^{3+} reduction. Experimentally, such reductive decomposition was reported by Dodd, where o-$FePO_4$ was found to be stable up to 400 °C in an inert atmosphere.[8] Upon further heating, o-$FePO_4$ was found to undergo irreversible phase transformation to non-olivine mixed-valent $(Fe_3^{2+}Fe_4^{3+})(PO_4)_6$, $Fe_2P_2O_7$ and t-$FePO_4$ phases.[8] Recently, J. Kim *et al.* also observed $FePO_4$ decomposition into $Fe_2P_2O_7$, but with sarcopside $Fe_3(PO_4)_2$ as an intermediate phase.[15] We have reported formation of $Fe_7(PO_4)_6$ and t-$FePO_4$ phases upon o-$FePO_4$ heating above 550 °C in N_2.[16] On the other hand, under oxidizing atmosphere, Rousse *et al.* determined that o-$FePO_4$ irreversibly transforms to t-$FePO_4$ above 620 °C.[14]

However, some discrepancies exist with reported calorimetry experiments on o-$FePO_4$, indicating this phase is more energetically stable than its trigonal form contradicting the research findings previously mentioned.[17] In this same experiment, o-$FePO_4$ was determined to be stable up to 600 °C in inert atmosphere.[17] Although no physical characterization was performed after calorimetry testing, the endothermic event was associated with an irreversible olivine to trigonal phase transition.[17] In contrast, under similar conditions, our results indicate an exothermic transformation of o-$FePO_4$ to $Fe_7(PO_4)_6$ and t-$FePO_4$.[16]

Although $FePO_4$ has been reported to have a high thermal stability, its counterpart, $MnPO_4$, does not share the same fate.

[a]*Department of Chemistry and Materials Science and Engineering Program, Binghamton University, Binghamton, NY, 13902-6000, USA. E-mail: stanwhit@gmail.com*
[b]*Brookhaven National Laboratory, Upton, NY 11973, USA*
[c]*Chemistry Department, University of Cambridge, Lensfield Rd, Cambridge, CB2 1EW, UK*
[d]*Chemistry Department, Stony Brook University, Stony Brook, New York 11794-3400, USA*

† Electronic supplementary information (ESI) available: Included are room-temperature and high-temperature X-ray diffraction, X-ray absorption spectroscopy at Fe and Mn K-edges, ^{7}Li nuclear magnetic resonance data, scanning transmission electron microscopy with electron energy-loss spectroscopy, thermal gravimetric analysis, mass spectroscopy and differential scanning calorimetry of olivine phosphates. See DOI: 10.1039/c2jm33183g

This journal is © The Royal Society of Chemistry 2012

View Article Online

Published on 15 August 2012. Downloaded by Florida State University on 7/18/2024 8:35:07 PM.

For instance, S.-W. Kim *et al.* and Chen *et al.* have shown that o-$MnPO_4$ undergoes phase decomposition above 150 °C, evolving oxygen and heat in the process to form a pyrophosphate.[5,18] S.-W. Kim *et al.* proposed the following reaction:

$$2MnPO_4 \rightarrow Mn_2P_2O_7 + ½O_2.$$

However, the reported weight losses upon o-Li_xMnPO_4 decomposition are significantly higher than the 5.4 wt% this reaction suggests.[19,20] In 2010, oxygen potential diagrams, determined from first principle calculations by Ong *et al.*, confirm substantial O_2 evolution from o-$MnPO_4$ upon heating, as well as decreased thermal stability.[7]

More recently, the effects of particle size on the phase stability of Li_xMnPO_4 ($0 < x < 1$) were investigated using *in situ* X-ray diffraction methods.[21] It was reported that completely delithiated Li_xMnPO_4 ($x = 0$) having particle sizes above 200 nm were observed to decompose to $Mn_2P_2O_7$ under vacuum, in accordance with previous work.[5] However, under similar atmospheric conditions, particles below 200 nm underwent phase transformations to form a sarcopside phase, $Mn_3(PO_4)_2$,[22] and a P-rich amorphous phase above 250 °C; suggesting that particle size affects the phase transformation route of $MnPO_4$.

In the present work, the mechanism of thermal decomposition of $Fe_{1-y}Mn_yPO_4$ ($y = 0$, 0.2, 0.4, 0.6, 0.8, 0.9) has been investigated using temperature-controlled *in situ* X-ray diffraction (XRD) methods, as well as calorimetry and thermogravimetric techniques. When this paper was in the final stages of preparation, a paper by J. Kim *et al.* reporting *in situ* XRD data upon heating of $Li_xFe_{1-y}Mn_yPO_4$ under vacuum appeared.[15] The results reported are essentially consistent with ours for $x \approx 0$ and $y \leq 0.5$. The behaviour of Mn-rich compounds is more controversial. Our work emphasizes the role of reductive impurities, *i.e.* residual carbon and hydrogen from moisture exposure, in thermal behaviour of $Fe_{1-y}Mn_yPO_4$, which explains diverse results reported in the literature.

Experimental details

Olivine phase $LiFe_{1-y}Mn_yPO_4$ ($y = 0$, 0.2, 0.4, 0.6, 0.8, 0.9, 1.0) was synthesized using a solid-state method. The precursor materials, Li_2CO_3 (Fisher, 99.5%), $FeC_2O_4 \cdot 9H_2O$ (Aldrich, 99%), $MnCO_3$ (Aldrich, 99.9%) and $(NH_4)_2HPO_4$ (Fisher, 99.80%), were mixed in a 1 : 2 : 2 : 2 molar ratio, then ball-milled for 6 h. Precursor mixture was pre-heated to 350 °C for 8 h under He/H_2 atmosphere. Then, the sample was pelletized and sintered at 550 °C for 10 h under a He/H_2 atmosphere in order to prevent Fe^{2+}/Fe^{3+} oxidation. The resulting $LiFe_yMn_{1-y}PO_4$ powder was then chemically delithiated using ≥200% molar excess NO_2BF_4 (Aldrich, 99.5%) in excess acetonitrile (Fischer, 99.9%). This mixture then underwent rigorous magnetic stirring for no less than 3 days under a N_2 atmosphere. Resulting powder was suction filtered and rinsed with organic solvents to remove unwanted impurities. In addition, drying and storage of all samples in a desiccator was utilized to prevent moisture exposure.

A nanosized $LiFe_{1-y}Mn_yPO_4$ ($0.7 < y < 0.75$) sample was obtained from Primet Precision Materials, Inc. $Fe_{1-y}Mn_yPO_4$ materials derived from this sample by chemical and electrochemical delithiation will be referred to as nano-$Fe_{1-y}Mn_yPO_4$. The chemical delithiation was done as described above. For the electrochemical delithiation, the cathode materials were prepared by mixing 80% active material, 10% carbon black and 10% polyvinylidene fluoride (PVDF) with 1-methyl-2-pyrrolidinone solvent. The slurry formed was then cast onto an Al foil current collector before drying. The dried electrodes, of area 1.2 cm^2, containing 3 to 5 mg of active material were placed in 2325-type coin cells in a He-filled glove box with pure lithium foil (Aldrich, thickness 23 μm) as the counter and reference electrode, and Celgard 2400 as the separator. 1 M $LiPF_6$ in a 1 : 1 volume ratio of ethylene carbonate (EC) and dimethyl carbonate (DMC) (LP30 from EMIndustries) was used as the electrolyte. The cells were charged to 4.5 V galvanostatically at 0.01 mA, held at 4.5 V for 2 hours, and then disassembled in He glove box. Cathodes were washed in DMC and dried. Nano-$Fe_{1-y}Mn_yPO_4$ were kept in glove box to minimize moisture exposure.

The crystal structure was characterized using powder X-ray diffraction (PXRD), where data was collected on a Scintag XDS2000 θ–θ powder diffractometer equipped with a Ge(Li) solid state detector and CuKα sealed tube ($\lambda = 1.54178$ Å). Data were measured over the range of 10–80° 2θ with a step size of 0.02° and exposure of 10 s for structure refinement; the samples were rotated to minimize the effect of preferred orientation. *In situ* high-temperature X-ray diffraction analysis was performed at the National Synchrotron Light Source, beamline X7B, wavelength 0.3196 Å, with a heating rate of 5 °C min^{-1} under He or He/O_2 (further termed as O_2) flow connected to residual gas analyser. Samples obtained from Primet were also studied at beamline X18A, wavelength 0.6199 Å, upon heating at 5 °C min^{-1} in air. Rietveld refinements of the X-ray diffraction patterns were performed using the GSAS/EXPGUI package.[23,24] X-ray absorption (XAS) data at Fe and Mn K-edges was collected at National Synchrotron Light Source, beamline X23A2, a bending magnet beamline equipped with Si(311) monochromator. XAS data was processed using Athena software.[25]

^{7}Li solid-state NMR was performed on a Bruker spectrometer with a magnetic field of 4.7 T and the Larmor frequency is 77.49 MHz. A Bruker 1.8 mm HX magic angle spinning (MAS) double resonance probe was used with a MAS speed of 35 kHz. A $\pi/2$–τ–π–τ-acquisition spin echo pulse sequence was used with a pulse delay of 0.1 s, $\pi/2$ pulse length of 1.3 μs, and $\tau = 28.57$ μs. 1 M LiCl with ^{7}Li resonating at 0 ppm was used for chemical shift reference and pristine $LiFePO_4$ for quantification calibration.

Transmission electron microcopy (TEM), scanning TEM images and electron energy-loss spectroscopy (EELS) spectra were recorded at 200 kV in the JEOL2100F microscope equipped with a Gatan image filter (GIF) spectrometer. The spectra were recorded in both STEM mode for local analysis and diffraction mode for average information. The energy resolution is about 1.1 eV, as measured by the FWHM of the zero-loss peak. The Scanning Electron Microscopy (SEM) of Primet sample was done on ZeissSupra-55 field emission scanning electron microscope, operating at 10 kV.

Differential Scanning Calorimetry (DSC) testing was performed using a TA Instruments Q200 calorimeter under flowing N_2 (50 mL min^{-1}) at a heating rate of 5 °C min^{-1}. The Thermal Gravimetric Analysis (TGA) was conducted on a Perkin-Elmer

View Article Online

Published on 15 August 2012. Downloaded by Florida State University on 7/18/2024 8:35:07 PM.

TGA 7 instrument under flowing N_2 and O_2 at a heating rate of 5 °C min^{-1}. CH analysis was done at Atlantic Microlab.

Results and discussion

Structure and composition of $Fe_{1-y}Mn_yPO_4$ obtained by chemical delithiation

XRD indicates pure olivine phases for both pristine and delithiated series (Fig. S1†). The cell volume and lattice parameters are compared with prior work in Fig. 1 and S1,† respectively.[4,26] Our $Fe_{1-y}Mn_yPO_4$ samples show slight unit cell volume decrease when Mn content increases to 0.6 followed by cell volume increase at higher Mn content (Fig. 1). $Fe_{1-y}Mn_yPO_4$ reported by Yamada's group show slight cell volume increase up to $y = 0.6$ followed by irregular behaviour above that value. The discrepancy arises from the *c* lattice parameter change (Fig. S1(b)†), which is the smallest compared to *a* and *b* variations with Mn content.

We used X-ray absorption (XAS) spectroscopy and ^{7}Li solid state NMR to characterize the Fe and Mn oxidation states, quantify the residual Li amounts and identify local coordination, as possible causes of irregular cell volume change. X-ray absorption spectra confirm complete oxidation of Fe^{2+} to Fe^{3+} upon delithiation, while a slight shift of the Mn K-edge toward lower energies for $y = 0.6$, 0.8 and 0.9 indicates incomplete Mn^{2+} to Mn^{3+} oxidation at high Mn concentrations, suggesting incomplete delithiation (Fig. S2 and S3†). ^{7}Li NMR analysis confirms complete delithiation up to Mn substitution corresponding to $y = 0.4$; whereas, above this concentration, incomplete delithiation resulted in o-$Li_xFe_{1-y}Mn_yPO_4$ ($0 < x < 0.03$, $0.6 \leq y \leq 1$); the exact compositions are given in Table S1.† The observed NMR shifts (Fig. S4†) indicate lithium residing in Mn-rich environment. Despite the minute residual Li remaining post-delithiation, no additional o-$LiFe_{1-y}Mn_yPO_4$ phases were observed in XRD studies; consistent with a reported monophase region for its Li-deficient, o-$Li_xFe_{1-y}Mn_yPO_4$ ($0 \leq x \leq 0.03$), phase.[27]

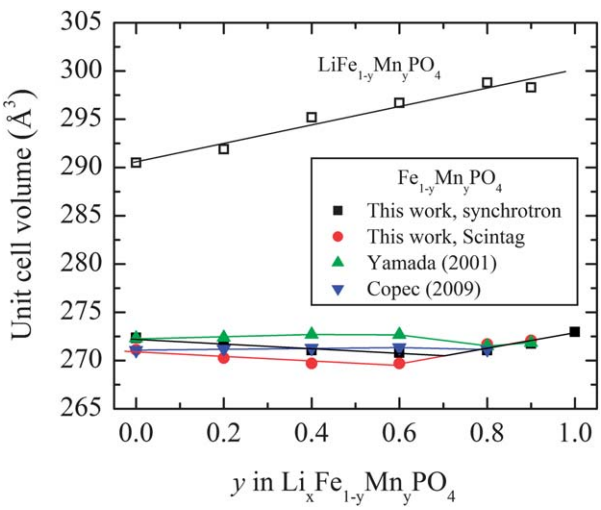

Fig. 1 Unit cell volumes of o-$LiFe_{1-y}Mn_yPO_4$ and chemically delithiated o-$Fe_{1-y}Mn_yPO_4$ as a function of Mn content *y*. Lines are given to guide the eye.

The CH analysis indicates 3–6 wt% of carbon remaining after decomposition of carbon-containing precursors and 0.1–0.3 wt% of hydrogen (Table S1†). The nature of hydrogen in these compounds and its role in thermal decomposition will be discussed later.

Transmission electron microscopy (TEM), supplemented with electron energy-loss spectroscopy (EELS) confirms complete delithiation of o-$FePO_4$, residual Li in o-$Li_{0.026}Fe_{0.1}Mn_{0.9}PO_4$ and determines particle size of this series to be approximately 100 nm, with some variation (Fig. 2 and S5†). We therefore attribute the cell volume increase for $y > 0.6$ to the incomplete delithiation due to large particle size.

Phase changes upon heating of $Fe_{1-y}Mn_yPO_4$ as evidenced by *in situ* XRD

In order to address discrepancies in o-$FePO_4$ thermal stability, we investigated its decomposition under both inert (N_2) and oxidizing (O_2) atmospheres. In our experiments, *in situ* X-ray diffraction was used to observe structural transformations in real-time upon heating at 5 °C min^{-1} to enable direct comparison with TGA and DSC data. Phase analysis of the XRD patterns presented in Fig. S6† indicate decomposition of o-$FePO_4$ to mainly $Fe_7(PO_4)_6$ under inert conditions above 600 °C and to single-phase t-$FePO_4$ at temperatures above 600 °C in O_2. These results suggest that the oxidative environment prevents the formation of a mixed-valent product ($(Fe_3^{2+}Fe_4^{3+})(PO_4)_6$) and is consistent with previous reports.[14,16]

o-$Fe_{0.8}Mn_{0.2}PO_4$ and o-$Fe_{0.6}Mn_{0.4}PO_4$ both show structural stability up to 600 °C under inert atmospheric conditions (Fig. 3 and S7(a)†). In addition, samples containing Mn do not show tendencies to form trigonal, t-$Fe_{1-y}Mn_yPO_4$, phases in XRD analysis at high temperatures. Both $y = 0.2$ and $y = 0.4$ samples reveal small XRD peak at 3 degrees 2θ between 600 °C and 700 °C, characteristic of sarcopside $M_3(PO_4)_2$ (M = Fe, Mn) phase.

However, the sarcopside phase eventually forms a major pyrophosphate phase, $(Fe,Mn)_2P_2O_7$, above 700 °C for $y = 0.2$ and above 650 °C for $y = 0.4$. A small amount of $M_7(PO_4)_6$ phase is evident above 700 °C by small XRD peaks between 2 and 3 degrees 2θ, and the olivine phase persists as minor phase.

When the Mn content is increased to $y = 0.6$ and above, structural changes are observed at temperatures as low as 250–300 °C. Namely, some of the olivine phase XRD peaks become broader and eventually split when the temperature increases

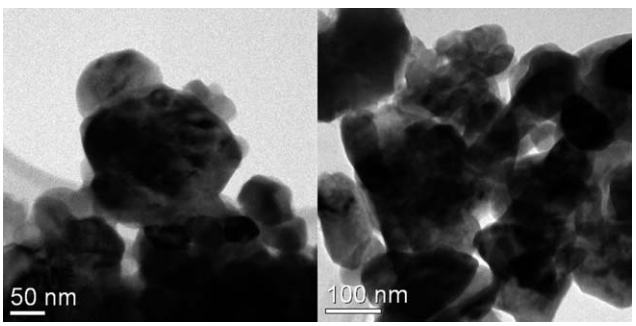

Fig. 2 Bright-field TEM images of (left) o-$FePO_4$ and (right) o-$Fe_{0.6}Mn_{0.4}PO_4$.

 This journal is © The Royal Society of Chemistry 2012

View Article Online

Published on 15 August 2012. Downloaded by Florida State University on 7/18/2024 8:35:07 PM.

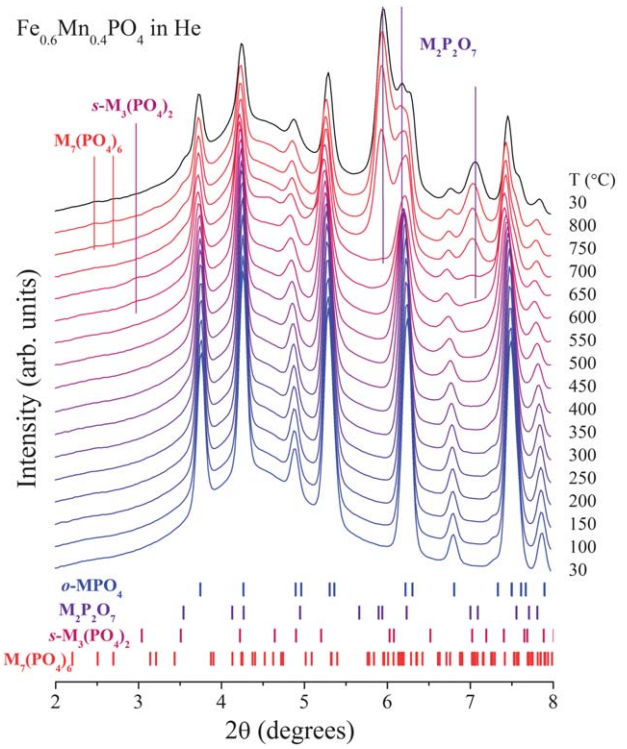

Fig. 3 *In situ* XRD data while heating o-$Fe_{0.6}Mn_{0.4}PO_4$ under inert atmospheric conditions.

(Fig. 4, 5 and S7(b)†). At $y = 0.6$, it is the most noticeable for (020) peak at 6.2 2θ degrees and (311) peak at 7.5 2θ degrees; while for $y = 0.8$ and 0.9, the (200) peak at 3.8 2θ degrees splits the most. The newly formed low-angle peaks fit best with $LiFe_{1-y}Mn_yPO_4$ structure, however the residual Li amount does not exceed 3 mol% (Table S1†), which is not enough to form such strong XRD peaks. Interestingly, o-$FePO_4$ also shows minor (200) peak broadening and splitting between 300 and 400 °C in both N_2 and O_2 atmospheres (Fig. S8†), confirming that this effect is neither entirely due to residual Li present at high Mn content nor due to oxygen loss.

Upon heating, o-$Fe_{0.4}Mn_{0.6}PO_4$ shows sarcopside peaks between 550 and 700 °C, while the pyrophosphate peaks first clearly appear at 650 °C (Fig. 4), similarly to the compounds with lower Mn content. o-$Fe_{0.2}Mn_{0.8}PO_4$ and o-$Fe_{0.1}Mn_{0.9}PO_4$ show pronounced (200) peak broadening and splitting between 250 and 400 °C; above this temperature, sarcopside phase appears, coexisting with the olivine, and persists up to 600 °C (Fig. 5 and S7(b)†). Above 600 °C both compounds transform into a mixture of pyrophosphate and $M_7(PO_4)_6$ phases.

We set up to check whether an O_2 atmosphere would prevent reduction of Mn-rich o-$Fe_{1-y}Mn_yPO_4$ upon heating, similarly to the effect observed for o-$FePO_4$, and conducted an *in situ* XRD study of heating o-$Fe_{0.1}Mn_{0.9}PO_4$ in O_2. According to Fig. 6, o-$Fe_{0.1}Mn_{0.9}PO_4$ shows the same (200) peak splitting when heated in O_2 as observed in He. Conversely, the sarcopside phase is not obvious in O_2, and the compound maintains its major olivine phase till 650 °C when heated in oxidizing conditions. After heating above 650 °C, XRD patterns indicate the formation of a pyrophosphate; suggesting oxidizing environment

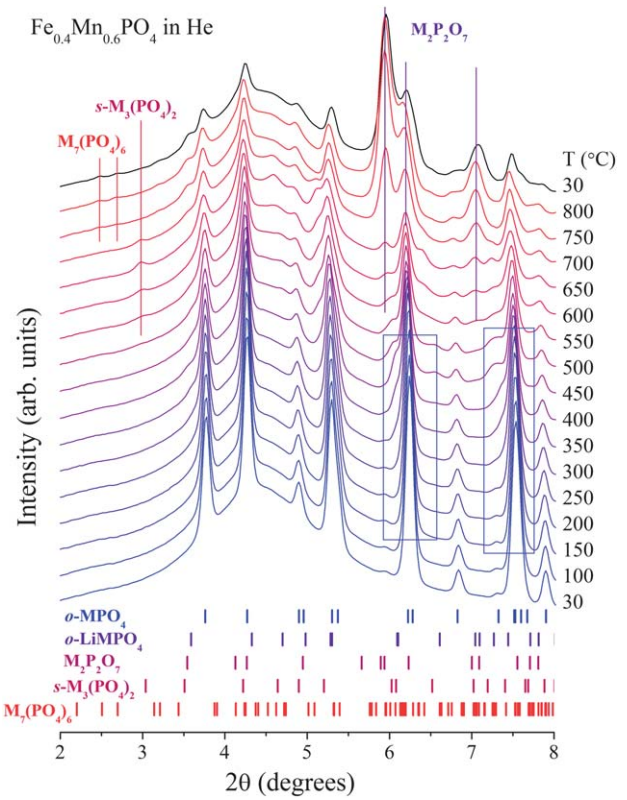

Fig. 4 *In situ* XRD data while heating o-$Fe_{0.4}Mn_{0.6}PO_4$ under inert atmospheric conditions. Frames highlight peak broadening.

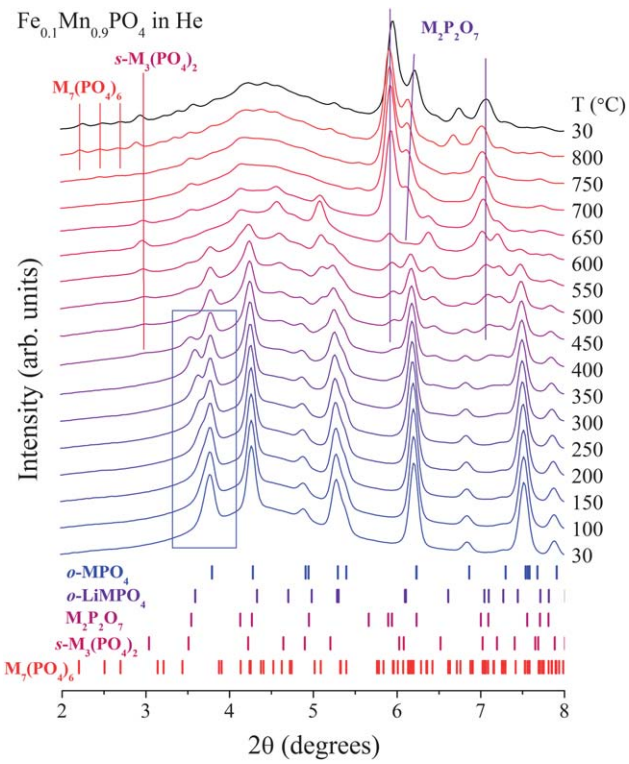

Fig. 5 *In situ* XRD data while heating o-$Li_{0.026}Fe_{0.1}Mn_{0.9}PO_4$ under inert atmospheric conditions. The frame highlights peak splitting area.

View Article Online

Published on 15 August 2012. Downloaded by Florida State University on 7/18/2024 8:35:07 PM.

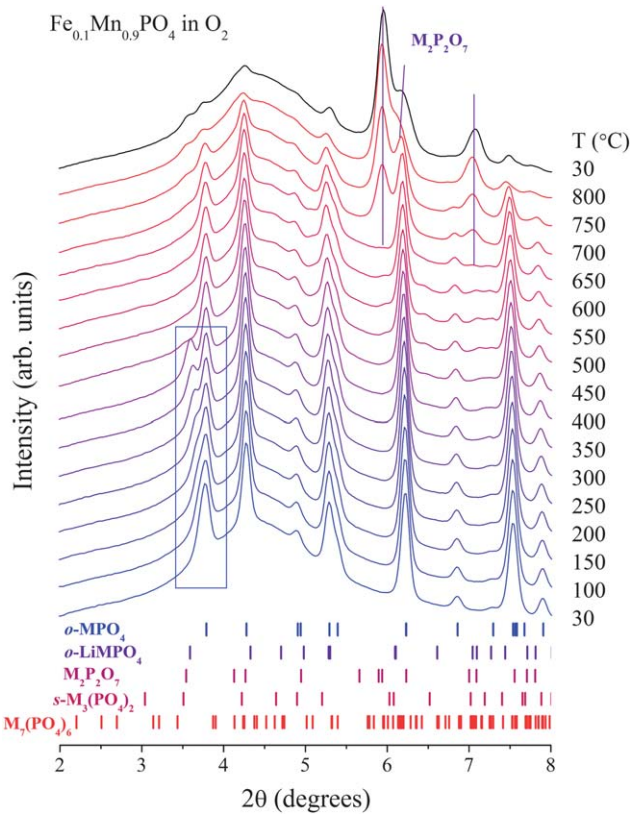

Fig. 6 *In situ* XRD data while heating o-$Li_{0.026}Fe_{0.1}Mn_{0.9}PO_4$ under oxidizing atmospheric conditions. The frame highlights peak splitting area.

suppresses the formation of a sarcopside phase at low temperatures, but does not prevent the high-temperature reduction. Interestingly, small olivine peaks are still observed, even at 800 °C, indicating slow kinetics of olivine to pyrophosphate transformation.

Structural changes and thermal analysis of $Fe_{1-y}Mn_yPO_4$

Rietveld refinement of the *in situ* XRD data was performed to determine the o-$Fe_{1-y}Mn_yPO_4$ unit cell parameters change upon heating. In case of phase coexistence, multiple phase refinement was used with phase compositions described above. The refinements reveal that the unit cell of the o-$Fe_{1-y}Mn_yPO_4$ increases linearly with temperature up to 300 °C, while above this temperature the dependence is also linear, but with a higher slope (Fig. 7). Therefore we have calculated two sets of thermal expansion coefficients α corresponding to the high- and low-temperature regions for each composition and heating atmosphere (Fig. 8). In the low-temperature region, α increases slightly from 2 to 3 × 10^{-5} K^{-1} with Mn content increase. The high-temperature values of α behave less regularly. At Fe-rich and Mn-rich ends of the o-$Fe_{1-y}Mn_yPO_4$ series these values are only slightly larger than the low-temperature ones, while for the intermediate compositions ($0.2 \leq y \leq 0.6$) the difference is larger, and in this composition range α decreases linearly with Mn content. Also, for the $0.2 \leq y \leq 0.6$ composition range, the olivine phase cell volume decreases above 600 °C (Fig. 7), that is, when the pyrophosphate phase starts to form. Multiple-phase

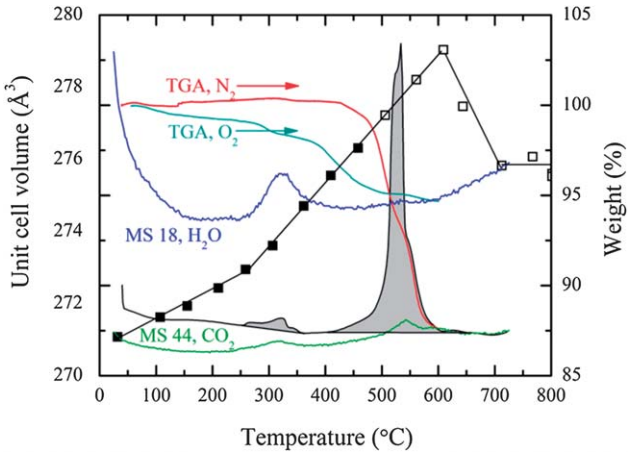

Fig. 7 Thermal and structural data for $Fe_{0.6}Mn_{0.4}PO_4$ combining TGA in nitrogen and oxygen, MS signals upon heating in N_2 for H_2O and CO_2 in arbitrary units on the same scale for both, DSC in N_2 with shaded areas corresponding to 15 J g^{-1} around 300 °C and 350 J g^{-1} between 450 and 600 °C. Unit cell volume of the olivine phase as a function of temperature is presented using solid squares if pure olivine phase is observed and in open squares when olivine coexists with sarcopside and/or pyrophosphate phases.

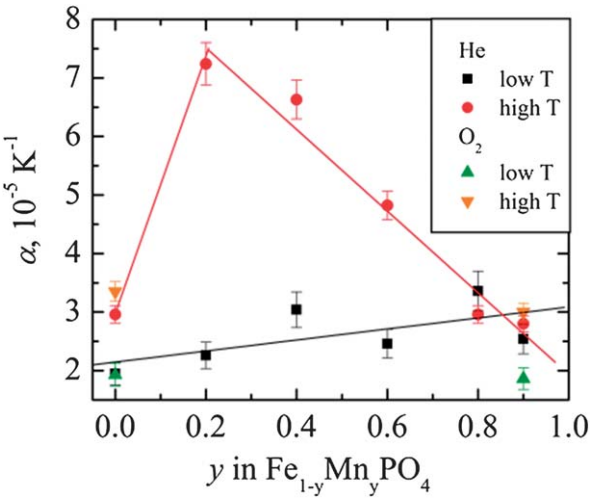

Fig. 8 Thermal expansion coefficients of o-$Fe_{1-y}Mn_yPO_4$ over low-temperature, $T < 300$ °C, and high-temperature, $300 < T < 500$ °C, regions.

Rietveld refinement of the post-heat products indicates that the cell volume of the resulting pyrophosphate phase is nearly constant for $0.4 \leq y \leq 0.9$ in o-$Fe_{1-y}Mn_yPO_4$ and corresponds to $(Fe_{0.3}Mn_{0.7})_2P_2O_7$, assuming that Vegard's law is applicable to the $(Fe_{1-y}Mn_y)_2P_2O_7$ series.[28,29] Correspondingly, the remaining olivine and mixed-valent $M_7(PO_4)_6$ phases should be Fe-rich, which explains why the olivine phase is observed at high temperatures even in Mn-rich o-$Fe_{1-y}Mn_yPO_4$.

Thermal gravimetric analysis (TGA) of o-$Fe_{1-y}Mn_yPO_4$ ($y \leq 0.6$) indicates that in O_2 the weight loss is about 5–7% consistent with oxygen loss due to partial reduction and residual carbon loss. In N_2, the weight loss is typically larger and attains 18% in some samples (Fig. 7 and S9†). Mass-spectrometry (MS) data

 This journal is © The Royal Society of Chemistry 2012

View Article Online

Published on 15 August 2012. Downloaded by Florida State University on 7/18/2024 8:35:07 PM.

conducted along with the TGA indicates H_2O and CO_2 evolution at 300 °C, meaning that excessive weight loss in N_2 is due to reductive action of residual carbon and hydrogen in the samples (see Table S1† for CH analysis data). In this case carbon and hydrogen bind with structural oxygen causing its removal from the structure upon heating, which results in higher weight loss compared to heating in O_2. At higher Mn contents, $y \geq 0.8$, the weight losses in either N_2 or O_2 are very large, 25–30%, majorly occurring above 400 °C, that is during the sarcopside phase formation. We are investigating the possibility of P loss due to phosphorous oxide sublimation, which is consistent with partial amorphization occurring upon heating of Mn-rich $Fe_{1-y}Mn_yPO_4$, as a likely cause of large weight loss.

Differential scanning calorimetry (DSC) under inert atmosphere indicates major exothermic peaks above 400 °C for $y \leq 0.4$ (Fig. 7 and S9†), evolving 310 and 350 J g^{-1} of heat for $y = 0.2$ and 0.4, respectively. The events at 300 °C, namely the thermal expansion coefficient change, H_2O and CO_2 evolution, are accompanied by small peaks in DSC varying from exothermic to endothermic in various samples. This suggests that at least two events occur at that point. We propose that the first one is the oxygen loss from the structure as evidenced by the MS data, and the second one is transition metal migration to former Li site, which we perceive as responsible for the XRD peak splitting. The disordered olivine phase, $M_\delta M_{1-\delta}PO_4$, so formed has larger lattice parameters,[30] so the shoulders form at low-angle side of the ordered olivine phase XRD peaks. Under inert atmospheric conditions this disordered phase transforms to the sarcopside at 400 °C, which is structurally related to olivine as $[\square_{1/2}M_{1/2}]MPO_4$, with M^{2+} and vacancies ordered at Li site of the olivine structure.[31] Under the oxidative conditions, transition metal reduction is delayed, so that sarcopside phase does not form, and the disordered phase seems to merge back with the ordered olivine phase above 400 °C (Fig. 6). The structural disorder and oxygen loss, eventually resulting in sarcopside phase formation, may be triggered by H^+ incorporation into the structure and its removal upon heating. In the next section we address this issue by studying how nano-$Fe_{1-y}Mn_yPO_4$ prepared by different methods decompose upon heating.

Thermal stability of moist and dry nano-$Fe_{1-y}Mn_yPO_4$ obtained by chemical and electrochemical delithiation

Cathode materials in Li-ion cells are delithiated electrochemically, and this process may result in slightly different structure than chemical delithiation. Moreover, good electrochemical performance at high currents requires nano-sized olivine phosphates, especially Mn-rich ones showing poorer performance at high current rates than $LiFePO_4$. Less thermal stability is expected of 20–50 nm particles because of higher area of less ordered surface. For the same reason, nano-particles are expected to be more hygroscopic. With this in mind we investigated thermal stability of nano-$Fe_{1-y}Mn_yPO_4$ ($0.7 < y < 0.75$) obtained by electrochemical and chemical delithiation of $LiFe_{1-y}Mn_yPO_4$ ($0.7 < y < 0.75$) with particle size below 50 nm (Fig. S10†). For this study, the *in situ* XRD was conducted in both moist (air) and inert (He) atmospheres.

Chemically delithiated sample with minimal air exposure shows excellent thermal stability (Fig. 9). Peak splitting is not observed in this case, only some peak broadening onsets at 400 °C. The sarcopside peaks first appear at 450 °C and the relative intensities of these peaks are comparable to those observed in $Fe_{1-y}Mn_yPO_4$ ($y = 0.8, 0.9$) with larger particle sizes (Fig. 6, S7(b)†), suggesting that the particle size is not the critical factor in sarcopside phase formation. Upon further heating, the olivine and sarcopside phases coexist until they convert to the pyrophosphate above 650 °C. Electrochemically delithiated sample is not that stable (Fig. 10). It shows peak broadening and splitting at 200 and 250 °C, respectively, and then the olivine phase completely converts to the sarcopside by 400 °C, which converts to the pyrophosphate by 600 °C.

The phase transformations of chemically and electrochemically delithiated nano-samples upon heating in naturally moist air are similar to each other, and to the electrochemically delithiated sample heated in helium. Nano-samples exposed to moisture show XRD peak splitting at 150 °C and 200 °C for electrochemical and chemical delithiation, respectively (Fig. 11 and 12). Above 250 °C both samples convert to the sarcopside phase, which transforms to the major pyrophosphate phase by 500 °C with minor $M_7(PO_4)_6$ phase present in post-heat products. This data indicate that moisture exposure catalyses the formation of sarcopside phase, as suggested above. In case of the electrochemically delithiated sample heated in helium, protons or other reductive species could enter the structure upon side reactions at high voltage. Nanosized samples convert to the sarcopside more easily because they have larger surface area and incorporate protons in the structure more readily. We propose the following equation for the catalytic action of incorporated protons:

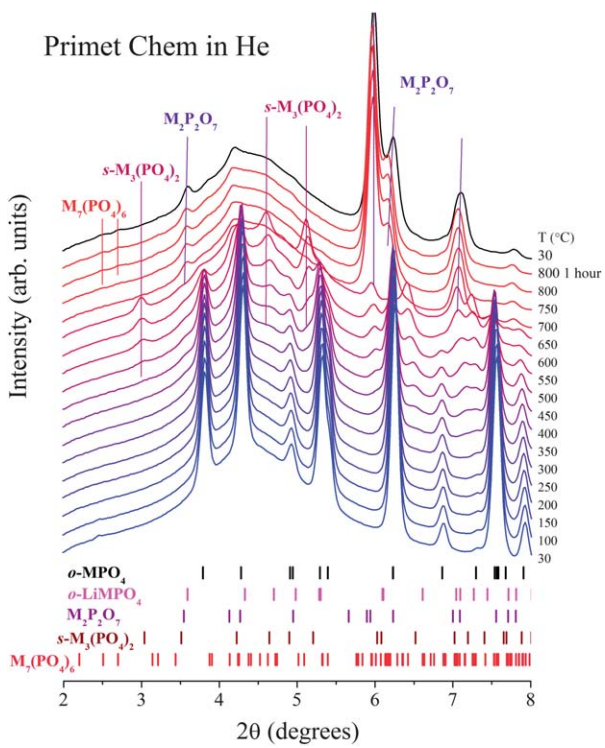

Fig. 9 *In situ* XRD data while heating in helium nano-$Fe_{1-y}Mn_yPO_4$ ($0.7 < y < 0.75$) obtained by chemical delithiation of Primet sample.

View Article Online

Published on 15 August 2012. Downloaded by Florida State University on 7/18/2024 8:35:07 PM.

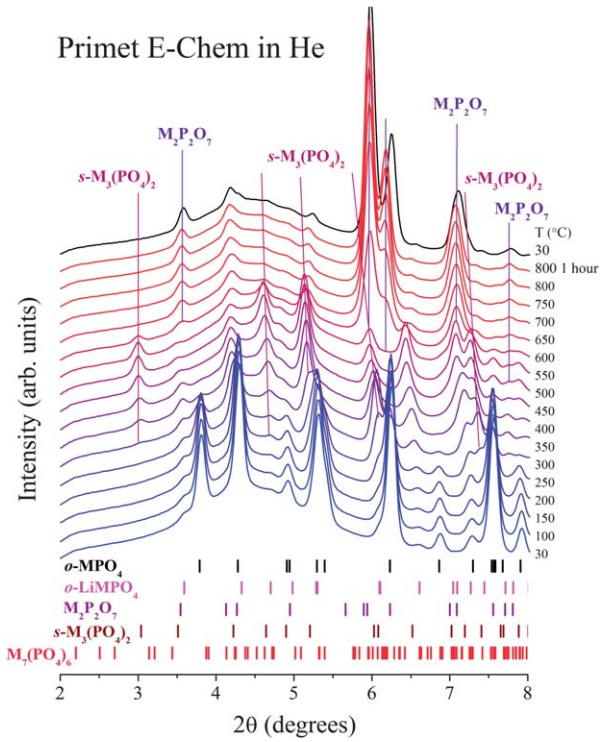

Fig. 10 *In situ* XRD data while heating in helium nano-$Fe_{1-y}Mn_yPO_4$ ($0.7 < y < 0.75$) obtained by electrochemical delithiation of Primet sample.

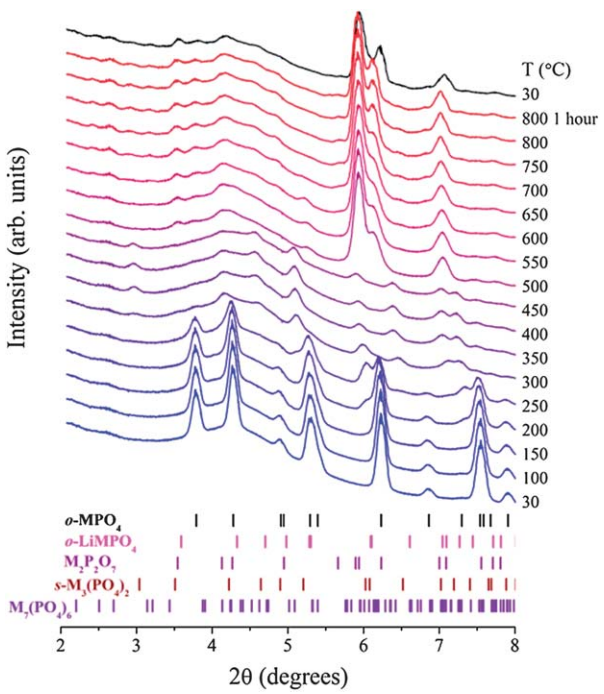

Fig. 11 *In situ* XRD data while heating in air nano-$Fe_{1-y}Mn_yPO_4$ ($0.7 < y < 0.75$) obtained by chemical delithiation of Primet sample. The pattern is recalculated to 0.3196 Å wavelength to ease comparison with previous datasets.

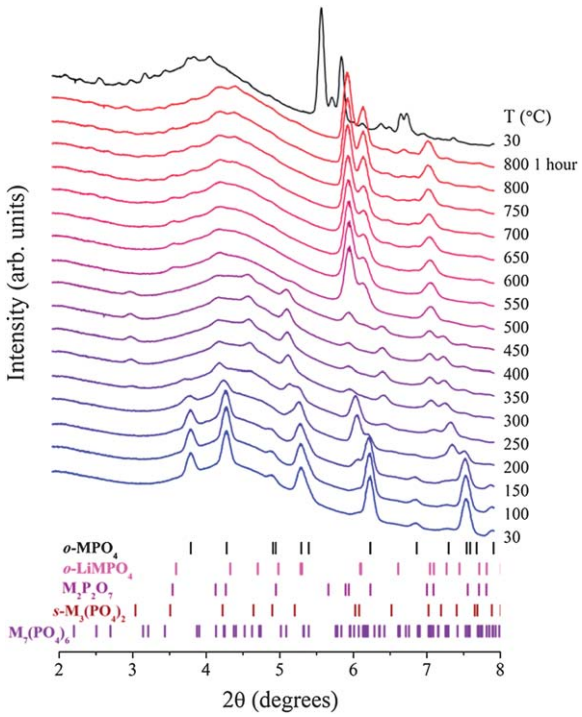

Fig. 12 *In situ* XRD data while heating in air nano-$Fe_{0.25}Mn_{0.75}PO_4$ ($0.7 < y < 0.75$) obtained by electrochemical delithiation of Primet sample. The pattern is recalculated to 0.3196 Å wavelength to ease comparison with previous datasets.

$$6\text{“}H_zFe_{1-y}Mn_yPO_4\text{”} \rightarrow 2z(Fe_{1-y}Mn_y)_3(PO_4)_2 + zP_2O_5 + 3zH_2O + 6(1-z)Fe_{1-y}Mn_yPO_4$$

Water formed as a result of this process induces further formation of the hydrated phase until all the olivine phase is converted to sarcopside. At this point, the structure of the moisture-exposed phase termed “$H_zFe_{1-y}Mn_yPO_4$” is not known, and is a subject of our current research. Hydrogen incorporation into the olivine structure is reported for olivine silicate minerals, where it seems to form hydroxyl group, and therefore can be expected for olivine phosphates as well.[32]

Conclusions

Olivine phase $Fe_{1-y}Mn_yPO_4$ appears to be stable up to at least 400 °C for Mn content up to $y = 0.9$ and particle size down to below 50 nm, when not exposed to moisture. Different thermal stabilities and decomposition routes reported in the literature and observed in this work, such as formation of $Fe_7(PO_4)_6$ or $Fe_2P_2O_7$ or t-$FePO_4$ upon heating of o-$FePO_4$ and $Mn_2P_2O_7$ or s-$Mn_3(PO_4)_2$ formation upon heating of o-$MnPO_4$ can be explained by reductive actions of carbon and hydrogen almost unavoidably present in the samples. Hydrogen incorporation into the $Fe_{1-y}Mn_yPO_4$ structure upon moisture exposure, demonstrated here by the TGA-MS data, appears the most detrimental to the thermal stability of Mn-rich samples ($y \geq 0.6$). It induces structural disorder as low as 150–200 °C leading to the sarcopside phase formation by 400 °C. The structure of the hydrogen-containing phase is being investigated.

 This journal is © The Royal Society of Chemistry 2012

View Article Online

Published on 15 August 2012. Downloaded by Florida State University on 7/18/2024 8:35:07 PM.

Acknowledgements

This research is supported as part of the NorthEastern Center for Chemical Energy Storage, an Energy Frontier Research Center funded by the U.S. Department of Energy, Office of Science, and Office of Basic Energy Sciences under Award Number DE-SC0001294. Use of the National Synchrotron Light Source at Brookhaven National Laboratory is supported by the U. S. Department of Energy, Office of Science, Office of Basic Energy Sciences, under Contract DE-AC02-98CH10886. Use of TEM facilities at the Center for Functional Nanomaterials, Brookhaven National Laboratory, is supported by the U.S. Department of Energy, Office of Basic Energy Sciences, under Contract No. DE-AC02-98CH10886. We thank Archit Lal and Robert Dobbs of Primet Precision Materials, Inc. for providing nano-$LiFe_{1-y}Mn_yPO_4$ sample for this work, and we would like to extend our gratitude to Archit Lal for stimulating discussions and helpful suggestions.

Notes and references

1 A. Padhi, K. Nanjundaswamy and J. Goodenough, *J. Electrochem. Soc.*, 1997, **144**, 1188.
2 M. S. Whittingham, *Chem. Rev.*, 2004, **104**, 4271.
3 G. Li, H. Azuma and M. Tohda, *Electrochem. Solid-State Lett.*, 2002, **5**, A135.
4 A. Yamada and S.-C. Chung, *J. Electrochem. Soc.*, 2001, **148**, A960.
5 S.-W. Kim, J. Kim, H. Gwon and K. Kang, *J. Electrochem. Soc.*, 2009, **156**, A635.
6 M. E. Arroyo y de Dompablo, N. Biskup, J. M. Gallardo-Amores, E. Moran, H. Ehrenberg and U. Amador, *Chem. Mater.*, 2010, **22**, 994.
7 S. Ong, A. Jain, G. Hautier, B. Kang and G. Ceder, *Electrochem. Commun.*, 2010, **12**, 427.
8 J. Dodd, PhD dissertation, California Institute of Technology, 2007.
9 G. Rousse, J. Rodriguez-Cravajal, S. Patoux and C. Masquelier, *Chem. Mater.*, 2003, **15**, 4082.
10 W. Eventoff, R. Martin and D. Peacor, *Am. Mineral.*, 1972, **57**, 67.
11 H. N. Ng and C. Calvo, *Can. J. Chem.*, 1975, **53**, 2064.
12 Y. Song, P. Zavalii, M. Suzuki and M. S. Whittingham, *Inorg. Chem.*, 2002, **41**, 5778.
13 S. Yang, Y. Song, P. Zavalij and M. S. Whittingham, *Electrochem. Commun.*, 2002, **4**, 239.
14 G. Rousse, J. Rodriguez-Carvajal, S. Patoux and C. Masquelier, *Chem. Mater.*, 2003, **15**, 4082.
15 J. Kim, K.-Y. Park, I. Park, J.-K. Yoo, J. Hong and K. Kang, *J. Mater. Chem.*, 2012, **22**, 11964.
16 G. M. Nolis, N. A. Chernova, S. Upreti and M. S. Whittingham, *MRS Online Proc. LIbr.*, 2011, **1333**, mrss11-1333-m03-03.
17 R. Iyer, C. Delacourt, C. Masquelier, J.-M. Tarascon and A. Navrotsky, *Electrochemical and Solid-State Letters*, 2006, **9**, A46.
18 G. Chen, A. Shukla, X. Song and T. Richardson, *J. Mater. Chem.*, 2011, **21**, 10126.
19 G. Chen and T. Richardson, *J. Electrochem. Soc.*, 2009, **156**, A756.
20 G. Chen and T. Richardson, *J. Power Sources*, 2010, **195**, 1221.
21 J. Kim, K.-Y. Park, I. Park, J.-K. Yoo, D.-H. Seo, S.-W. Kim and K. Kang, *J. Electrochem. Soc.*, 2012, **159**, A55.
22 J. Warner, A. Cheetham, A. Nord, R. Vondreele and M. Yethiraj, *J. Mater. Chem.*, 1992, **2**, 191.
23 B. H. Toby, *J. Appl. Crystallogr.*, 2001, **34**, 210.
24 A. C. Larson and R. B. VonDreele, *General Structure Analysis System (GSAS)*, Los Alamos National Laboratory Report LAUR, 2000, vol. 86, p. 748.
25 B. Ravel and M. Newville, *J. Synchrotron Radiat.*, 2005, **12**, 537.
26 M. Kopeć, A. Yamada, G. Kobayashi, S. Nishimura, R. Kanno, A. Mauger, F. Gendron and C. M. Julien, *J. Power Sources*, 2009, **189**, 1154.
27 A. Yamada, H. Koizumi, N. Sonoyama and R. Kanno, *Electrochem. Solid-State Lett.*, 2005, **8**, A409.
28 P. F. Henry, M. T. Weller and C. C. Wilson, *J. Appl. Crystallogr.*, 2003, **36**, 1361.
29 T. Stefanidis and A. G. Nord, *Acta Crystallogr., Sect. C: Cryst. Struct. Commun.*, 1984, **C40**, 1995.
30 J. Chen, M. J. Vacchio, S. Wang, N. Chernova, P. Y. Zavalij and M. S. Whittingham, *Solid State Ionics*, 2008, **178**, 1676.
31 P. B. Moore, *Am. Mineral.*, 1972, **56**, 2445.
32 M. Hirschmann and D. Kohlstedt, *Phys. Today*, 2012, **65**(3), 40; S. Demouchy and S. Mackwell, *Phys. Chem. Miner.*, 2006, **33**, 347.